Earth Science Informatics (2025) 18:263
https://doi.org/10.1007/s12145-025-01776-2

RESEARCH

Designing a deep learning-based framework for the prediction of lake surface closed curves

Celso Augusto Guimarães Santos[1] · Debasmita Misra[2] · Sophia Ghanimeh[3] · Adeyemi Olusola[4] · Utkarsh Patel[5] · Golmar Golmohammadi[6] · Erfan Abdi[7] · Vahid Karimi[7] · Mohammad Ali Ghorbani[7]

Received: 11 October 2024 / Accepted: 4 February 2025

Abstract

Predicting the surface area and shape of lakes is critical for ecological, hydrological, and climatic studies. Accurate predictions enhance the understanding of lake dynamics, facilitate water resource management, and support environmental change assessments. Traditional methods, while foundational, often lack the efficiency, accuracy, and scalability required to handle complex lake systems, necessitating modern, technology-driven approaches. This study introduces a novel methodology for predicting changes in lake surface area and shape, including shoreline dynamics. The approach employs advanced remote sensing techniques and mathematical modeling, integrating Mathematica simulations with Net-Encoder and Deconvolution models. The framework achieved a high accuracy rate of 93% in water pixel extraction. Results indicate significant reductions in surface area, with Lake Eucumbene shrinking by 4.3% and the Salton Sea by 14.54%. The most notable shoreline changes occurred in the southwestern and northern regions of Lake Eucumbene and the southwestern region of the Salton Sea. This research highlights the effectiveness of a remote sensing-based approach for monitoring lake surface dynamics, offering a low-cost, high-accuracy tool for environmental monitoring and climate change impact assessment. Compared to existing methods, the proposed approach provides equivalent accuracy while delivering enhanced operational simplicity and flexibility.

Keywords Environmental monitoring · Infrared imaging · Shoreline dynamics · Satellite data · Water body delineation

Communicated by Hassan Babaie.

✉ Celso Augusto Guimarães Santos
celso@ct.ufpb.br

✉ Sophia Ghanimeh
s.ghanimeh@qu.edu.qa

✉ Mohammad Ali Ghorbani
ghorbani@tabrizu.ac.ir

Debasmita Misra
dmisra@alaska.edu

Adeyemi Olusola
aolusola@yorku.ca

Utkarsh Patel
utkarshp@iitbhilai.ac.in

Golmar Golmohammadi
g.golmohammadi@ufl.edu

Erfan Abdi
erabdi78@gmail.com

Vahid Karimi
vahid.karimi@tabrizu.ac.ir

1 Department of Civil and Environmental Engineering, Federal University of Paraíba, João Pessoa, Paraíba 58051-900, Brazil

2 Department of Civil, Geological and Environmental Engineering, University of Alaska Fairbanks, P.O. Box 755900, Fairbanks, AK 99775-5900, USA

3 Environmental Science Center, Qatar University, Doha, Qatar

4 Faculty of Environmental and Urban Change, York University, Toronto, Canada

5 Indian Institute of Technology, IIT Bhilai Main Campus, Bhilai, Kutelabhatha, Durg, Chhattisgarh 491001, India

6 Department of Soil, Water and Ecosystem Sciences, University of Florida, Gainesville, FL, USA

7 Department of Water Engineering, University of Tabriz, Tabriz, Iran

Published online: 17 February 2025

Introduction

Closed curves and their applications

Closed curves are looping shapes without specific starting or ending points, characterized by their ability to enclose defined areas. These curves are useful mathematical tools for representing real-world phenomena that exhibit closed-loop patterns, such as orbits, circuits, and boundaries (Abbena et al. 2017). Over the years, closed curves have been increasingly applied across various fields, including detecting tumor contours in medicine (Gu et al. 2014), modeling geological structures in geology (de Kemp and Sprague 2003), analyzing plant leaf shapes in botany (Laga et al. 2014), and studying urban development boundaries in urban planning (Zheng et al. 2018). Their ability to represent geographical features and analyze complex systems has made them particularly valuable in hydrological studies for modeling and predicting patterns within lake systems (Keren 2004).

Environmental monitoring and the role of lakes

Environmental monitoring aims to detect changes over time in specific areas, such as the degradation of inland water bodies caused by anthropogenic activities. These activities include land use changes, agricultural expansion, water diversion by dams, sewerage infrastructure development, and pollution (Kingsford et al. 2016). Lakes are critical components of local water cycles and are especially significant in arid regions where they provide both ecological and economic benefits. Consequently, sustainable monitoring and timely intervention are crucial to managing these vital freshwater resources effectively.

Remote sensing tools for monitoring lakes

Remote sensing (RS) has emerged as a cost-effective and scalable tool for monitoring surface water changes. RS methods reduce the need for extensive fieldwork and offer advantages such as wide spatial coverage, high-frequency data availability, and rich informational content (Ozesmi and Bauer 2002; Asokan and Anitha 2019). However, challenges remain in estimating and predicting spatiotemporal variations across large geographic areas and understanding the factors driving these changes, such as rainfall, temperature, and evaporation (Emami and Zarei 2021). When integrated with Geographic Information Systems (GIS) and Global Positioning Systems (GPS), RS enables the efficient monitoring of dynamic changes in lake systems (Wang et al. 2023). Numerous satellite sensors have been used for mapping and monitoring water surface areas, including the Advanced Very High-Resolution Radiometer (AVHRR) (Holben 1986), Moderate Resolution Imaging Spectroradiometer (MODIS) (Li et al. 2013; Feng et al. 2019), *Systeme Probatoire d'Observation de la Terre* (SPOT) (Harvey and Hill 2001), Visible Infrared Imaging Radiometer Suite (VIIRS) (Li et al. 2018), Landsat (Mueller et al. 2016; Chen et al. 2018; Wang et al. 2020), and Sentinel-2 (Du et al. 2016; Yang et al. 2017). Among these, the Landsat program stands out for its long-term, free, and continuous datasets dating back to 1972, with a temporal resolution of 16 days (Feyisa et al. 2014).

Advances and limitations of traditional methods

Various methods have been developed for water body analysis, including single-band approaches, spectral relationship analyses, water indices, object-oriented methods, decision trees, Support Vector Machine (SVM), Back Propagation (BP) neural networks, and deep learning-based methods (Santos et al. 2024). Notable tools include the Normalized Difference Water Index (NDWI), introduced by McFeeters (1996), and its refinement, the Modified NDWI (MNDWI), which improved the index's accuracy (Han-Qiu 2005). Further contributions include the Composite Index of Water Body (CIWI) by Ma et al. (2009) and the Automatic Water Extraction Index (AWEI) by Feyisa et al. (2014), which accounts for shadow conditions through two variants: AWEIsh for shadowed areas and AWEInsh for unshadowed areas. These methodologies have significantly advanced the field but face limitations in handling complex and dynamic systems such as lakes, particularly when predicting future changes in surface area and shoreline dynamics. Table 1 provides a comparative overview of studies that have employed these technologies to analyze lake surface areas, highlighting the evolution of methodologies over time and their application across different regions.

Research gap and study objectives

Despite these advancements, relatively few studies have focused on predicting the future spatial dynamics of lake surfaces (Abdi et al. 2024). For instance, Bakr and Abd El-kawy (2020) used the Land Change Modeler (LCM) based on the statistical Markov Chain method, which assumes memorylessness and oversimplifies complex systems. In contrast, this study adopts a robust methodology combining deep learning, binary classification, and deconvolution techbiques to simulate water surface changes, including future area variations and directional shoreline changes. Research utilizing closed curves for lake surface predictions remains limited (Shang 2013; Liu et al. 2021a), particularly for lakes such as Lake Eucumbene in Australia and the Salton Sea in the United

Table 1 Comparison of different research in this field

Lake-Region	Purpose of the research	Time series	Index and model used to detect water body	Reference
Al-Razzaz-Iraq	Analyzing Spatiotemporal changes in the area of the lake	1988–2018	NDVI[1], NDMI[2], NDWI[3], WI[4]	(Al-lami et al. 2023)
Aral-Central Asia	Geospatial quantitative analysis for volume and area of the lake	1987–2018	NDWI, NSM[5], LRR[6]	(Wu et al. 2022)
Siling Co, Zhuo Nai, Qinghai -Tibetan Plateau	Analysis of the annual map of lakes	1991–2018	MNDWI[7], NDVI, EVI[8]	(Zhao et al. 2022)
Alpine Lakes- Changtang Plateau	Recent dynamics of lake changes	2009–2014	NDWI, HRWI[9]	(Yang et al. 2017)
Nainital-India	Investigating the changes in the Water Spread Area Changes	2001–2018	NDWI, MNDWI, WRI[10]	(Deoli et al. 2022)
Glacial lakes- Tibetan Plateau	Investigating the spatial and temporal evolution of glacial lakes	1990–2019	MNDWI, NDWI	(Dou et al. 2021)
Dalinor, Chahannur, Angulinao, Huangqihai, Daihai-Mongolian plateau	Analyzing changes in lake surface area (LSA) and shrinkage risk	2000–2019	NDVI, NDWI	(Wang et al. 2022)
Toshka-Egypt	Monitoring the trend of area, volume, and water level of the lake	1998–mid2017	NDLI[11], ELI[12]	(Chipman 2019)
Dongting-china	Investigating the relationship between land use /land cover (LULC) change and land surface temperature (LST) in the lake area	1952–2010	NDVI, NDMI	(Tan et al. 2020)
Chad-African	Relationship between land surface temperature and lake area changes	1988–2016	Radar	(Policelli et al. 2018)
Qilu-China	Examining time-spatial changes of lake area	2000–2020	NDVI, MNDWI, $AWEI_{sh}$[13]	(Wang et al. 2023)
Lake > 1km^2- Qilian Mountains	Investigating the dynamics of the lake to climate change	1990–2020	NDWI	(Zhao et al. 2023)
Sarygamysh- Central Asia	Investigating the spatial changes of the lake area	1973–2022	SVM[14]	(COSTACHE, 2023)
Nuntasi Tuzla -Romany	Detection of lake surface water changes	1984–2021	NDVI, MNDWI, WNDWI[15], WRI	(Şerban et al. 2022)
Burdur, Egirdir, Beysehir-Turkey	Investigating the relationship between temporal-spatial changes and lake surface water temperature (LSWT)	2000–2021	NDWI, NDVI	(Albarqouni et al. 2022)
Bhimtal, Sattal, Naukuchiatal-India	Area survey and water distribution mapping	2001–2018	NDWI, MNDWI, WRI, NDVI	(Deoli et al. 2021)

(1) Normalized Difference Vegetation Index, (2) Normalized Difference Moisture Index, (3) Normalized Difference Water Index, (4) Water Index, (5) Net Shoreline Movement, (6) Linear Regression Rate, (7) Modified Normalized Difference Water Index, (8) Enhanced Vegetation Index, (9) High Resolution Water Index, (10) Water ratio index, (11) Normalized difference lake index, (12) Enhanced lake index, (13) Automated Water Extraction Index, (14) Support Vector Machine, and (15) Weighted Normalized Difference Water Index

States, where most studies focus on data prior to 2018 (Wu et al. 2022; Zhao et al. 2022; Al-lami et al. 2023).

This study examines spatiotemporal variations in water surface areas and predicts future changes in two distinct bodies of water: Lake Eucumbene in Australia and the Salton Sea in the United States. The methodology includes: (1) mapping open water bodies using Landsat TM and OLI satellite images from 2000 to 2023; (2) applying a binary classification algorithm to extract closed curves, enabling accurate measurements of lake surface areas; (3) predicting future surface areas based on precipitation, temperature, and water level data; and (4) analyzing closed curves to assess shoreline changes and comparing predictions with historical data. This integrated approach leverages advanced machine learning models to provide a low-cost, high-accuracy solution for monitoring and predicting fluctuations in lake surface areas.

Materials and methods

Simulation techniques

Shape delineation

The mathematical properties of closed curves have facilitated advancements in medical imaging techniques, structural engineering designs, and theoretical mathematics, underscoring their versatility and significance in both practical applications and research (Fig. 1). Their distinctive charactheristics—such as high flexibility, precise boundary definition, and simplified modeling—make them invaluable tools for simulating complex phenomena.

In this research, closed curve forecasting was used to model the evolution of the natural systems under study, specifically focusing on shape analysis, which has been demonstrated to be a reliable approach in similar applications. To optimize accuracy, this study applied a binarization method, which involves categorizing pixel values into two distinct groups based on a predefined threshold (Mundus et al. 2025). Pixels below the threshold were assigned a value of 0, while those above were assigned a value of 1. This binary classification enhances the identification and analysis of image features, facilitating more accurate curve fitting and improving the detection and classification of visual objects (Howe 2013).

Scale adjustment

In this study, the pixel surface area was determined using a scale adjustment process, which involved (1) calculating the Euclidean distance (ED) between two points on the

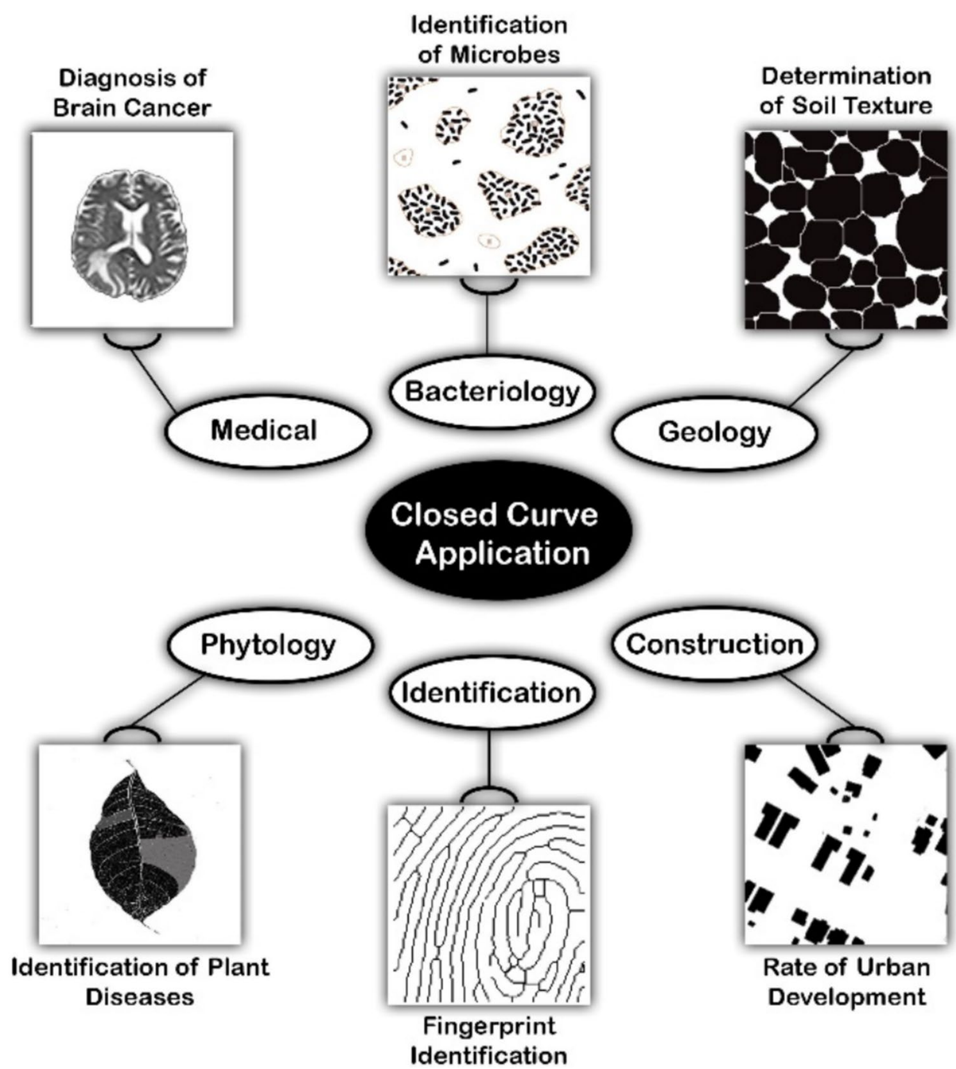

Fig. 1 Examples of closed curve applications

scale (Eqs. 1 and 2), and (2) computing the pixel surface area (Eq. 3). The total surface area of the lake (in km²) is then calculated by multiplying the area of each pixel by the total number of pixels within each closed curve. Euclidean distance, a fundamental concept in geometry and data analysis, represents the straight-line distance between two points in Euclidean space. It is widely applied in various fields, including machine learning, computer vision, and clustering algorithms (Wang et al. 2005).

$$\mathrm{ED} = \sqrt{(\mathrm{a}-\mathrm{x})^2 + (\mathrm{b}-\mathrm{y})^2} \tag{1}$$

$$\text{Scale Factor} = \frac{\mathrm{ED}}{\mathrm{Sc}} \tag{2}$$

where Sc represents the actual scale of the image in square kilometers (km²).

$$\text{Pixel Area} = \frac{1}{\text{Scale Factor}^2} \tag{3}$$

This method allows for accurate surface area estimation by incorporating both pixel resolution and scale adjustments, which are essential for modeling the areas of closed curves, such as lake surfaces. The schematic procedure for shape delineation and the scale adjustment method is illustrated in Fig. 2.

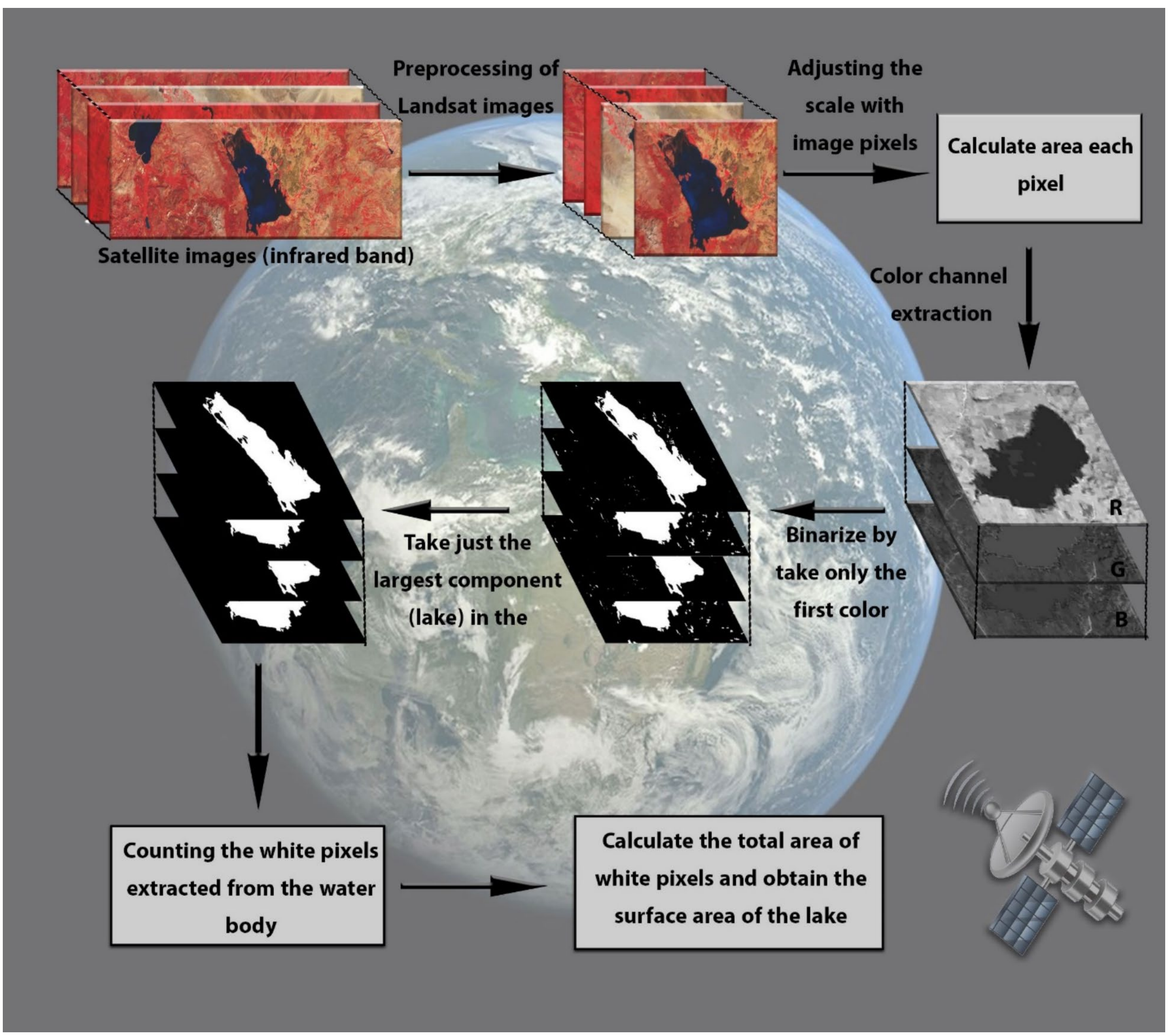

Fig. 2 Schematic representation of shape delineation and scale adjustment for computing lake surface area

Machine learning

The prediction of closed curves in this study was achieved through the application of machine learning techniques, where models were first trained to predict related parameters using deep learning approaches (Thornber and Williams 2000). Unlike traditional artificial neural network (ANN) models, deep learning architectures incorporate more advanced neurons and multiple layers, allowing for sophisticated operations such as convolutions. Additionally, these architectures enable the use of multiple activation functions within a single neuron, enhancing model performance (Hao et al. 2016; Rocio et al. 2017; Janiesch et al. 2021).

To forecast the lake surface area for the following year, the primary model utilized relevant accessible input data, including temperature, precipitation, and water level records from 2000 to 2023. The surface area served as the output variable. The structure and parameters of the deep learning model employed in this study are summarized in Table 2.

To address challenges commonly encountered in computer vision and image processing, such as object detection and boundary delineation, this study employed encoded deconvolution techniques. By encoding the input image into a lower-dimensional representation, the model was able to extract key features of the closed curves while reducing data complexity. The deconvolution process then reconstructed the closed curve from this encoded information, improving the accuracy of predictions. This approach not only enhances the precision of forecasting closed curves but also improves the overall effectiveness of computer vision applications.

Net encoder

In the context of neural networks, a net encoder serves as a fundamental tool for transforming non-numerical data into a numerical format, enabling subsequent processing by neural networks. In this study, the Wolfram Language was employed due to its advanced computational capabilities, including specialized encoders and decoders (Wolfram, 2024). A net encoder functions by taking an input dataset, characterized by an underlying but unknown probability distribution, and generating a multivariate latent encoding vector. The encoder models the data as a distribution defined by the network parameters. Equation (4) represents a key concept in generative models, particularly in the context of autoencoders and variational autoencoders (Liang et al. 2020):

$$P_{\theta}(x) = \int P_{\theta}(z)P_{\theta}(x|z)dz \tag{4}$$

where z represents the latent variable, x denotes the input data, and θ is the set of network parameters. The integral captures the encoding of the input data into a latent representation, facilitating the learning process within the neural network. This formula encapsulates the essence of how net encoders function within generative modeling frameworks, emphasizing their critical role in learning and sampling from complex data distributions (Hajizadeh Javaran et al. 2023).

Table 2 General information about deep learning layers

Model	Type of parameters	Values
Deep Learning	Network Type	Feed-forward propagation
	Data Division	Train (70%) Test (30%)
	Validation process	10-fold cross validation
	Number of Hidden layers (Neurons)	10
	Epoch number	1000
	Learning function	0.001–0.007
	Activation function	Relu
	Training function	Adam

Deconvolution neural network

This study employs deconvolution methods, an inverse operation to convolution, for signal and image processing. Deconvolution reconstructs the original signal from its convolution with a kernel or impulse response (Mulligan et al. 1995; Fanton 2021). The primary objective of deconvolution is to solve the convolution equation, which is typically achieved through statistical estimation methods or by applying the physical principles governing the underlying system (Sage et al. 2017). Processing speed and output quality are enhanced by reducing the number of iterations and accelerating convergence toward a stable estimate (Cornwell et al. 1999). This approach improves the signal-to-noise ratio and eliminates specific artifacts, making it particularly effective in signal and image processing applications. The output size of a deconvolution layer can be determined using a formula (Eq. 5) similar to that of a standard convolution layer, but with key differences. This formula, which accounts for the distinct mechanics of deconvolution, is provided by Press et al. (1992):

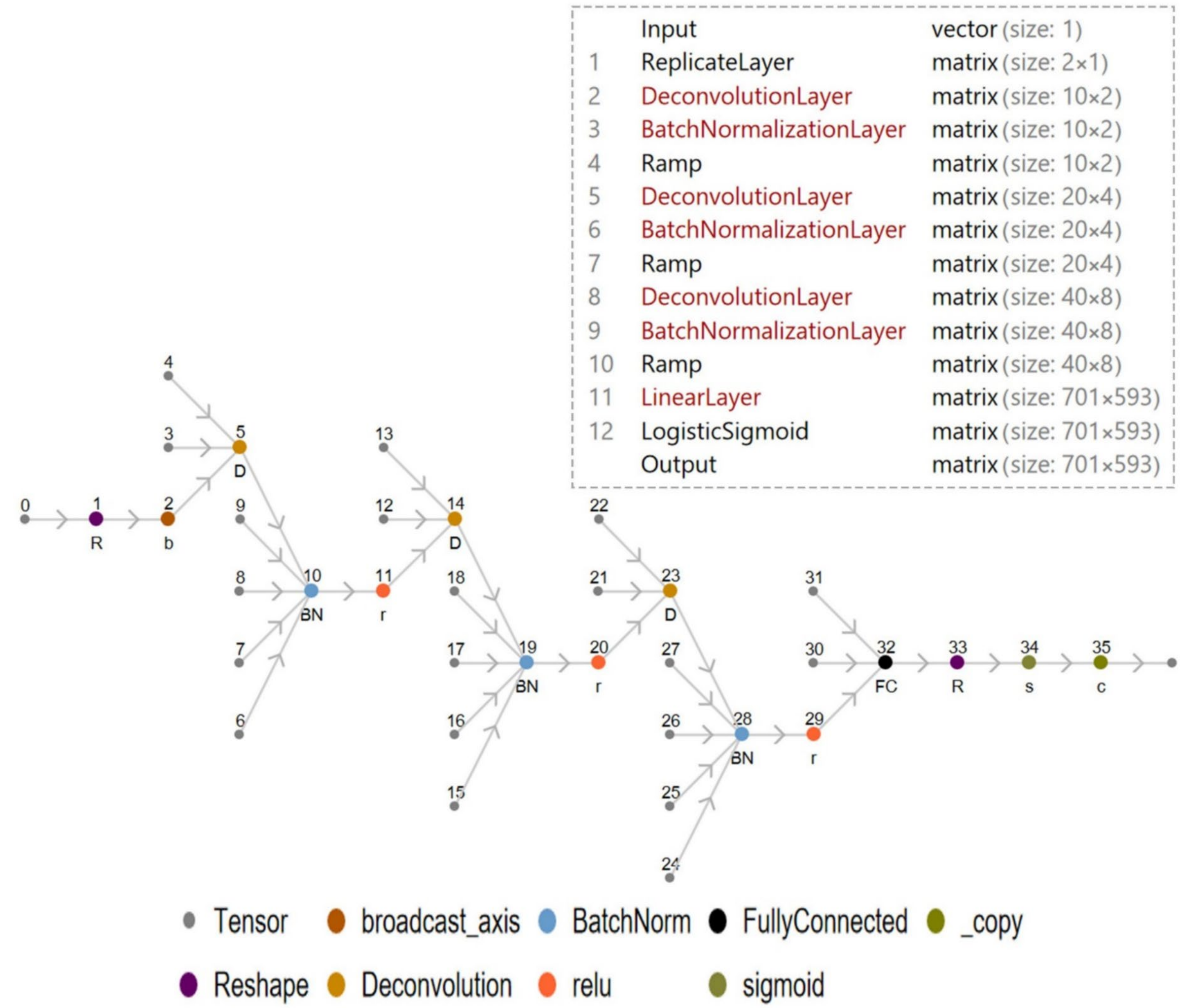

Fig. 3 Structure and parameters of the deconvolutional neural network developed for this study

$$\text{Output size} = \left\lfloor \frac{\text{input size} + 2 \times \text{ padding} - \text{dilation} \times (\text{kernel size} - 1) - 1}{\text{stride}} + 1 \right\rfloor \quad (5)$$

where the input size refers to the height or width of the input feature map, padding represents the number of pixels added around the input, the dilation rate defines the spacing between kernel elements, the kernel size denotes the height or width of the convolution kernel, and the stride determines the movement of the kernel. Figure 3 illustrates the architecture of the deconvolutional neural network utilized in this study.

Application to lake systems

Study areas

This research analyzes two lakes situated in distinct geographical regions: Lake Eucumbene in Australia and the Salton Sea in the United States. These sites were chosen for their contrasting geographical and climatic conditions, allowing the proposed methodology to be tested under diverse environmental settings (Fig. 4).

- **Lake Eucumbene** (36°12′S, 148°61′E), located approximately 40 km from Cooma in the Snowy Mountains of Australia, sits at an altitude of 1,200 m. The lake, with

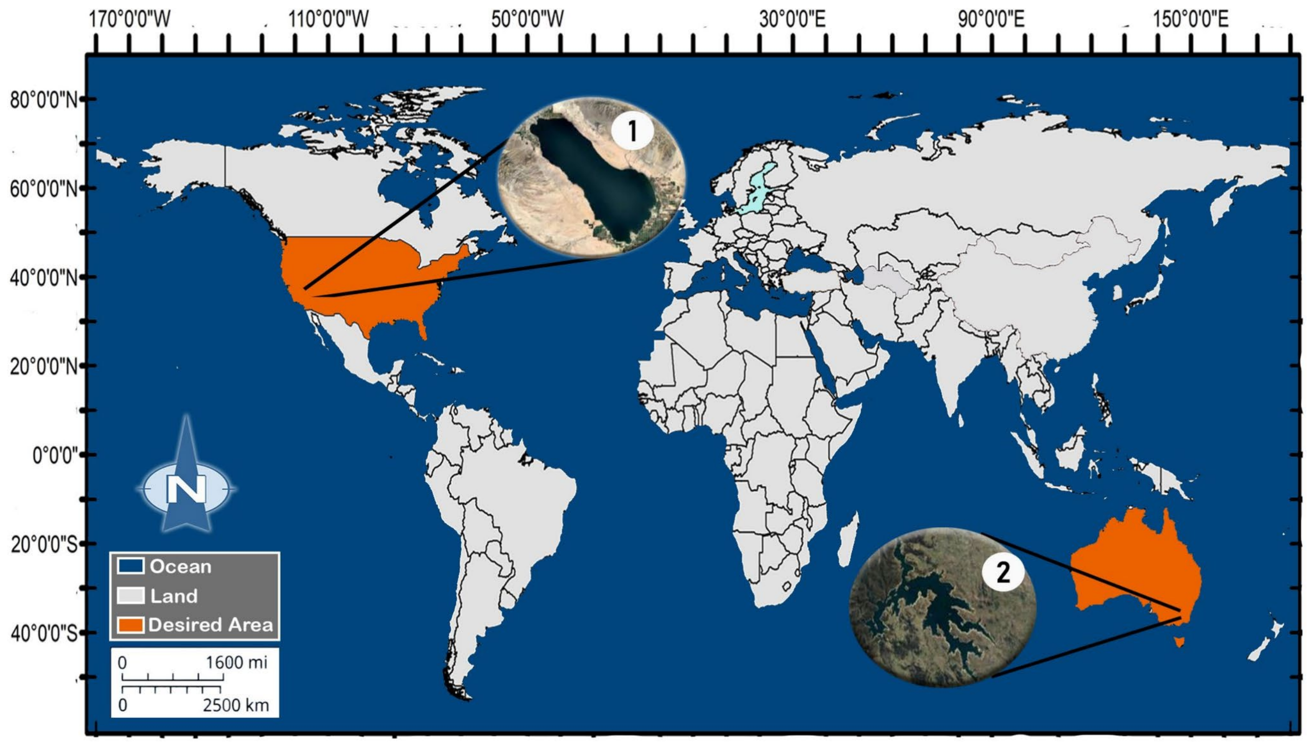

Fig. 4 Geographical locations of the study lakes: (1) Salton Sea, California, USA; and (2) Lake Eucumbene, New South Wales, Australia

Table 3 Characteristics of the study lakes (Wang et al. 2023; Wu et al. 2022)

Lake	Maximum extent (km²)	Type	Maximum depth (m)	Elevation (m)	Purpose of use
Eucumbene	145	Freshwater	107	1200	Irrigation, electricity generation
Salton	889	Brackish	13	−70	Irrigation, fisheries

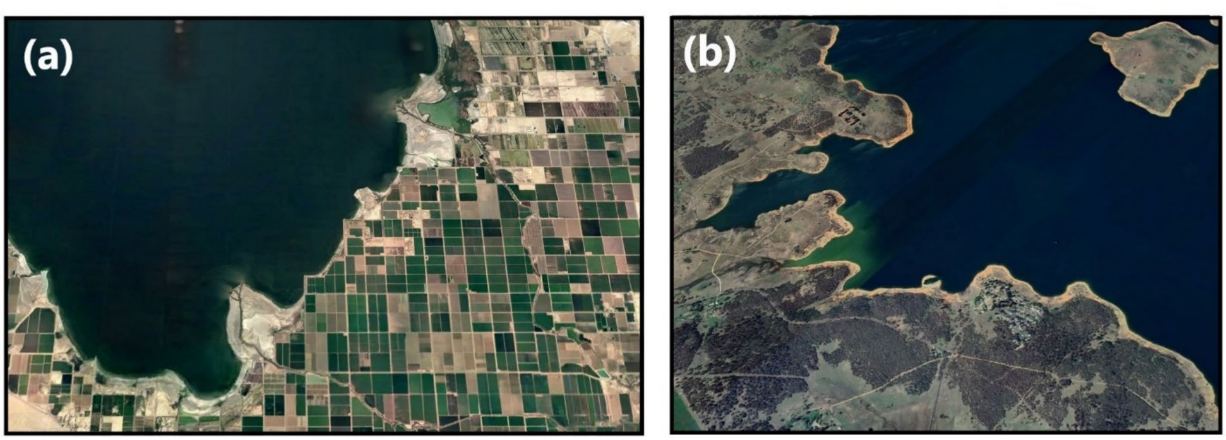

Fig. 5 Coastal configuration of selected bodies of water as viewed on Google Earth: **a** Salton Sea (USA), **b** Lake Eucumbene (Australia)

an average depth exceeding 30 m, experiences mild and stormy summers, along with cold and wet winters. Rainfall is relatively consistent throughout the year, peaking in late winter and spring.

- **The Salton Sea** (33°18′47″N, 115°50′04″W), a eutrophic, hypersaline, terminal lake in southeastern California, USA, is the largest inland water body in the state and serves as a crucial habitat for migratory birds. The average depth of the Salton Sea is 8 m, with a maximum depth of 13 m, situated approximately 70 m below sea level. The region experiences air temperatures ranging from 9 to 37 °C (Holdren 2014; Kjelland and Swannack 2018).

Each of these lakes possesses unique characteristics in terms of maximum extent, elevation, maximum depth, and other relevant attributes (Table 3). The coastlines of the Salton Sea and Lake Eucumbene (Fig. 5) exhibit agricultural lands and built structures along the southeast of Lake Eucumbene and the southwest of the Salton Sea. These landscapes could significantly affect these areas, emphasizing the importance of studying shoreline direction and transformations in relation to land use.

Data sources

Spatial and temporal resolutions are key factors in satellite imagery that significantly influence the ability to monitor and analyze changes on Earth's surface (Ozesmi and Bauer 2002). To analyze changes in the study areas from 2000 to 2023, a collection of 24 Landsat images per year, captured in September, was obtained for each lake from Landsat Look, under the supervision of the USGS (https://landsatlook.usgs.gov/explore). The spatiotemporal changes in Lake Eucumbene and the Salton Sea during this period were investigated using data from the Landsat Thematic Mapper (TM), Enhanced Thematic Mapper Plus (ETM+), and Operational Land Imager (OLI). To ensure precise analysis, images with minimal cloud cover (less than 10%) were selected, as excessive cloud cover can obscure the area of interest. Additionaly, to ensure smooth and clear imagery, four satellite sensors were employed: Landsat 5 TM (coverage from 1984 to 2013), Landsat 7 ETM+ (coverage from 1999 to 2023), Landsat 8 OLI/TIRS (coverage from 2013 to 2023), and Landsat 9 OLI+/TIRS (coverage from 2021 to 2023) (Albarqouni et al. 2022) (Table 4).

Table 4 Overview of the satellite imagery dataset used for analyzing both lakes

Sensors	Period	Number of images
Landsat 5	2000–2001	2
Landsat 7	2002–2007	6
Landsat 8	2008–2019	12
Landsat 9	2020–2023	4

For this study, data regarding the water levels and surface areas of the two lakes (Eucumbene and Salton) from 2000 to 2023 were sourced from the Database for Hydrological Time Series of Inland Waters (DAHITI) via the Hydroweb service (https://dahiti.dgfi.tum.de/en). Table 5 presents the statistical characteristics of three key parameters: precipitation, temperature, and water level for the studied lakes.

Study case simulation

The simulation of the lake systems using closed curves involves two main steps: (1) extracting the lake's closed curves from satellite images and estimating the surface area, and (2) forecasting the evolution of the lake's closed curves for the following year, followed by an analysis of the physical implications of the results.

- **Step one**

The initial step in the extraction process involved selecting satellite images with minimal cloud cover. To enhance the detection of the lakes' closed curves, the images were decomposed into individual RGB channels. This decomposition allowed for the analysis of each channel independently to identify the most effective one for representing the lakes' closed curves. It was determined that the red channel provided the clearest distinction of the closed curves compared to the other channels (Xiang et al. 2018; Ying and Lin 2019). Consequently, the red channel was selected for further binarization and analysis, enabling accurate delineation of the lakes' closed curves. The infrared images, shown in Fig. 6, were processed using Mathematica 13.3 software. Binarization of these images resulted in a binary format that

Table 5 Statistical characteristics of three important parameters of precipitation, temperature, and water level for four selected lakes

Lake	Temperature (C°)				Precipitation (cm)				Water level (m)			
	Max	Mean	Min	Num zero	Max	Mean	Min	Num zero	Max	Mean	Min	Num zero
Eucumbene	6.6	4.6	3	0	20.7	8.8	1.1	0	1152.5	1137.1	1123.3	0
Salton Sea	33.6	30.5	28.7	0	3.6	0.4	0	9	−69.2	−70.9	−73.1	0

effectively distinguishes lake pixels (white) from non-lake pixels (black) along the closed curves (Fig. 7).

Using an extraction algorithm based on the binary method, the closed curves representing the lake boundaries are derived from the images. Afterward, an appropriate scale is set, and the pixel area is calculated. The surface area of the lakes is then estimated based on the extracted closed curves.

- **Step two**

Machine learning was implemented through deep learning models using relevant parameters, such as network architecture, the number of hidden layers, and the number of epochs. Historical data was used to train these models. Subsequently, the image data was encoded to minimize the volume of computations and avoid unnecessary complexity. Finally, deconvolution modeling was applied to forecast and reconstruct the closed curves of the lakes for the following year.

Results and discussion

Lakes surface area delineation and future estimation

After scale adjustment and pixel analysis, the surface areas of the lakes were estimated from the extracted closed curves. To generate future forecasts, the primary model was configured to predict lake surface areas using air temperature, precipitation, and water level data as inputs, while the surface area served as the output variable.

The results demonstrated high reliability and precision in estimating the areas of the lakes, achieving coefficients of determination (R^2) of 0.96 for Lake Eucumbene and 0.98 for the Salton Sea, with root mean square errors (RMSE) of 4.107 km² and 1.259 km², respectively (Table 6). Compared to similar studies (Xu et al. 2021; Poudel et al. 2021), the method adopted in this study has proven to be equally accurate, yet operationally simpler and considerably more flexible.

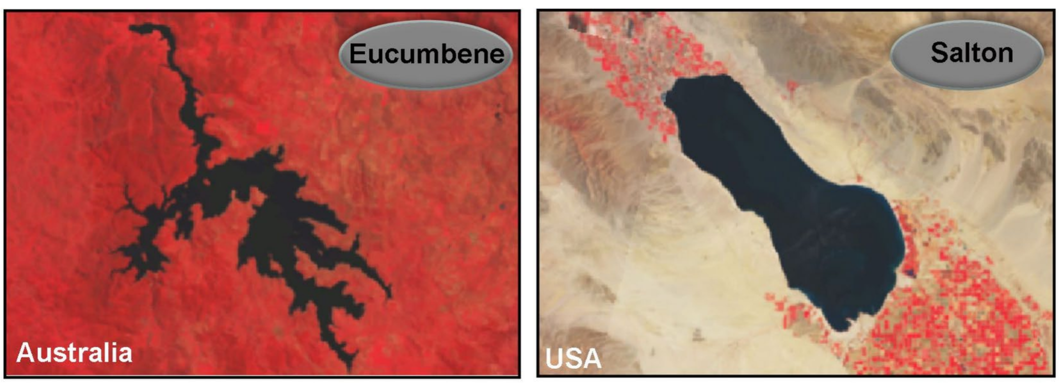

Fig. 6 Infrared imaging of the selected lakes

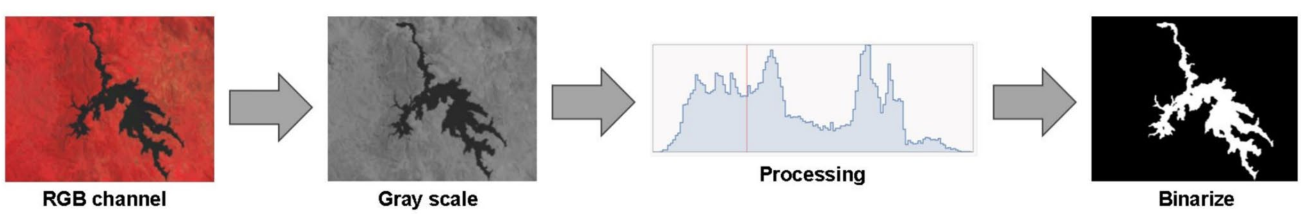

Fig. 7 Illustration of image binarization

Table 6 Accuracy assessment results of the estimated surface areas by water detection algorithm

Lake	Smallest area (km²)	Largest area (km²)	R^2	RMSE (km²)	Accuracy
Lake Eucumbene	47.82 (in 2007)	124.35 (in 2013)	0.960	4.107	84.0%
Salton Sea	827.15 (in 2022)	975.61(in 2001)	0.980	1.259	99.75%

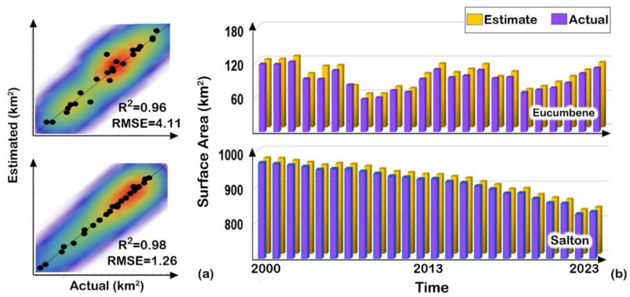

Fig. 8 Analysis of estimated lake surface areas: **a** scatter plots and **b** histogram for the studied lakes

Historical evolution

According to the estimates, the minimum and maximum surface areas for Lake Eucumbene were 47.82 km² in 2007 and 124.35 km² in 2013, respectively, while for the Salton Sea, the minimum and maximum surface areas were 827.15 km² in 2022 and 975.61 km² in 2001, respectively. The time series plots reveal an irregular pattern of changes in the water surface area of Lake Eucumbene and a gradual decreasing trend for the Salton Sea during the period 2000–2023 (Fig. 8). The plot for the Salton Sea is less scattered compared to Lake Eucumbene, indicating more consistent results.

Figure 9a shows the rate of change, at five-year intervals, for Lake Eucumbene. The largest expansion occurred during 2010–2015, at a rate of 61.85%, while the largest shrinkage occurred during 2005–2010, at 37.04%. The most significant changes in Lake Eucumbene occurred in the north, east, and south directions. Similar patterns were observed for Lake Tinaroo, located in Queensland, Australia, which also has a cool climate and abundant rainfall. The highest changes for Lake Tinaroo were observed in 2018, with a surface area reduction of 13.5% (Sumiya et al. 2020).

Figure 9b illustrates a gradual shrinkage of the Salton Sea, reaching a maximum of 5.10% between 2015 and 2020. The most significant changes occurred in the north, south, and southwest directions, where drying has posed environmental concerns for local populations. Similar findings were reported for the Great Salt Lake in northern Utah, another saline, endorheic basin, where a surface area decrease of approximately 6.56% was recorded in 2022 (Lang et al. 2023).

Using recent geometrical and coordinate data of Lake Eucumbene, a geometric map of the lake was developed (Fig. 10). Figure 10a illustrates substantial changes in Lake Eucumbene's coastline between 2000 and 2020, with the most significant alterations occurring in the northern section. Figure 10b shows a consistent annual decrease in the surface area of the Salton Sea, with 2020 marking the most substantial reduction. The greatest shrinkage occurred in the northeast and southern directions.

Forecasted changes

The Deconvolutional Neural Network model was implemented to detect a reliable correlation between lake surface areas and closed curve imagery. Table 7 presents the overall modeling accuracy and the associated errors in forecasting closed curve imagery. According to the table, the average accuracy for predicting the closed curves of the lakes is 97.9% for Lake

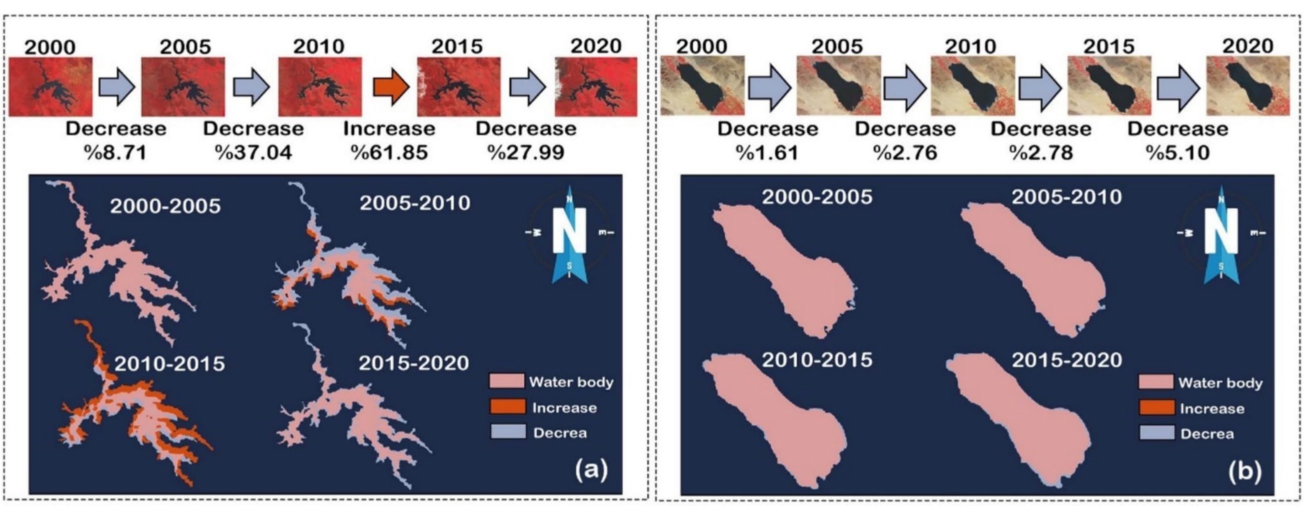

Fig. 9 Lake closed curves variations and directional changes (2000 to 2020): (i) water surface area changes and rates, based on Landsat imagery (in five-year intervals); and (ii) directional changes in the lake closed curves for (**a**) Eucumbene, and (**b**) Salton

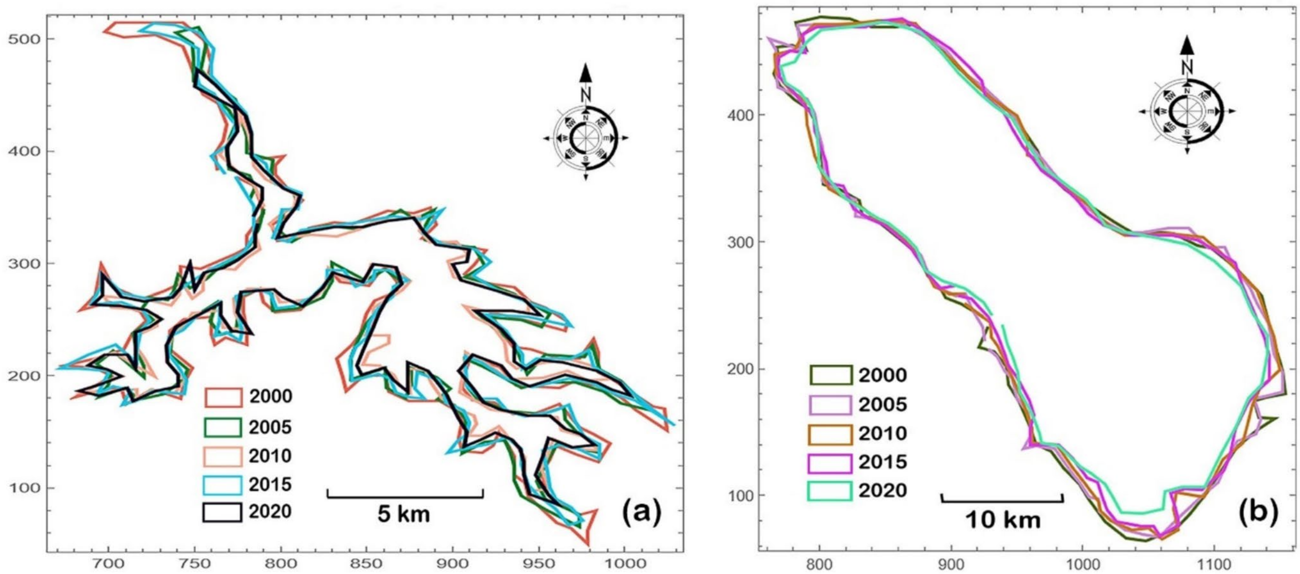

Fig. 10 Spatial changes in Lake (**a**) Eucumbene and (**b**) Salton, based on geometric and coordinate analysis

Table 7 Accuracy assessment results of the forecasted closed curves of the lakes

Lake	RMSE (km²)	*R*	Accuracy (%) (low, high)
Eucumbene	7.728	0.9869	(95.98, 99.82)
Salton	8.155	0.8553	(95.37, 99.45)

Eucumbene and 97.41% for the Salton Sea. Compared to previous research by Wang et al. (2024), which applied deconvolutional neural networks to detect landslides, the model demonstrates high robustness in imagery predictions.

According to the forecasts (Table 8), both lakes are expected to experience a decrease in surface area over the next year, with a reduction rate of 3.61% for Lake Eucumbene and 2.52% for the Salton Sea. The shrinkage of Lake

Table 8 Prediction of closed curves and rate of surface area changes for 2023–2024

	Closed curve (2023)	Closed curve (2024)	Changes (2023-2024)	Rate of Change (%)
Eucumbene	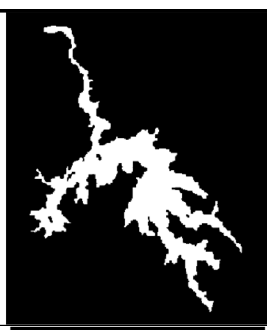	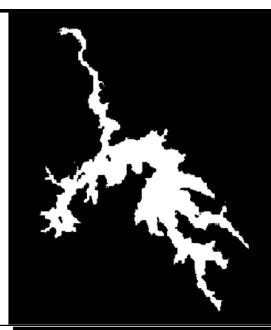		−3.609
Salton		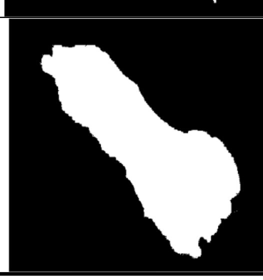	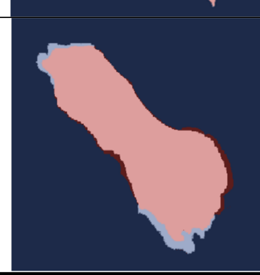	−2.522

Eucumbene is predicted to be most pronounced in the north and southeast regions, while the Salton Sea's reduction will be more noticeable in the northwest and southern regions.

The results can be attributed to the impacts of climate change on surface water resources. Overall, the lake surface predictions for both lakes in the next year align with the findings of previous studies. According to Liu et al. (2021b), projected rising temperatures and varied precipitation in the near future are expected to result in decreased surface flows, particularly during the dry season (April–September), across certain watersheds in California. Similarly, by 2030, a projected decrease in average rainfall, combined with increasing air temperatures and evaporation, is anticipated to exacerbate drought conditions in New South Wales, Australia (Hennessy et al. 2004; Srikanthan et al. 2022).

Conclusions

This study introduces a novel approach utilizing closed curves to forecast the evolution of lake surface areas, focusing on Lake Eucumbene and the Salton Sea as case studies. The results reveal significant historical shrinkage for both lakes; Lake Eucumbene experienced a maximum reduction of 50.92% in 2007 (compared to 2000) while the Salton Sea experienced a shrinkage of 15.21% in 2022. Predictions for the upcoming year indicate further declines in the surface areas of both lakes, with projected reductions of 3.60% for Lake Eucumbene and 2.52% for the Salton Sea, compared to 2023.

The high R^2 values and low RMSE across various stages of the modeling process demonstrate the accuracy and precision of the proposed methodology. The use of closed curves has proven effective for both interpreting historical trends and predicting short-term changes in the surface area and shape of lakes. Notably, the method provides a viable solution when data availability is limited, as it relies on machine learning techniques using readily accessible parameters, such as temperature, precipitation, and water levels.

Future studies should incorporate uncertainty analysis and examine the influence of more specific parameters, such as discharge flow rates, feeding flow rates, and evaporation, to further enhance the accuracy and applicability of the model. Including these additional factors may provide deeper insights into the dynamics of lake surface evolution and improve the predictive capabilities of the proposed approach. Furthermore, using a weekly to monthly time resolution for forecasting lake level changes could enable more effective monitoring of dynamic environmental conditions.

Author contributions Conceptualization: S. Ghanimeh, U. Patel , G. Golmohammadi , V. Karimi, M.A. Ghorbani; Methodology: C.A.G. Santos, D. Misra, U. Patel, G. Golmohammadi, E. Abdi, V. Karimi, M.A. Ghorbani; Formal analysis and investigation: All authors; Writing - original draft preparation: C.A.G. Santos, D. Misra, S. Ghanimeh, U. Patel, E. Abdi, V. Karimi; Writing - review and editing: S. Ghanimeh, A. Olusola, S. Sadeddin, G. Golmohammadi, V. Karimi; Resources: A. Olusola, M.A. Ghorbani; Supervision: S. Ghanimeh, G. Golmohammadi, M.A. Ghorbani; Reading and approving the final manuscript: All authors.

Funding No funding was received for conducting this study.

Data availability Data available on reasonable request.

Declarations

Competing interests The authors declare no competing interests.

References

Abbena E, Salamon S, Gray A (2017) Modern differential geometry of curves and surfaces with mathematica. Chapman and Hall/CRC

Abdi E, Ali M, Santos CAG et al (2024) Enhancing groundwater level prediction accuracy using interpolation techniques in deep learning models. Groundw Sustain Dev 26:101213. https://doi.org/10.1016/j.gsd.2024.101213

Albarqouni MMY, Yagmur N, Bektas Balcik F, Sekertekin A (2022) Assessment of spatio-temporal changes in water surface extents and lake surface temperatures using google earth engine for lakes region, Türkiye. ISPRS Int J Geoinf 11:407

Al-lami AK, Abbood RA, Al Maliki AA et al (2023) Using of different satellite-derived indices to detect the spatiotemporal changes of the Al-Razzaza Lake, Iraq. Iraqi J Sci 1030–1040

Asokan A, Anitha J (2019) Change detection techniques for remote sensing applications: a survey. Earth Sci Inf 12:143–160

Bakr N, Abd El-kawy OR (2020) Modeling the artificial lake-surface area change in arid agro-ecosystem: a case study in the newly reclaimed area, Egypt. J Environ Manage 271:110950. https://doi.org/10.1016/j.jenvman.2020.110950

Chen B, Chen L, Huang B et al (2018) Dynamic monitoring of the Poyang Lake Wetland by integrating Landsat and MODIS observations. ISPRS J Photogramm Remote Sens 139:75–87

Chipman JW (2019) A multisensor approach to satellite monitoring of trends in lake area, water level, and volume. Remote Sens (Basel) 11:158

Cornwell T, Braun R, Briggs DS et al (1999) Synthesis imaging in radio astronomy II. Astron Soc Pac 180:151–170

COSTACHE M-Ștefan (2023) The spatial dynamics of Sarygamysh Lake using remote sensing and GIS techniques. Cinq Continents 13

de Kemp EA, Sprague KB (2003) Interpretive tools for 3-D structural geological modeling part i: bézier-based curves, ribbons and grip frames. Geoinformatica 7:55–71. https://doi.org/10.1023/A:1022822227691

Deoli V, Kumar D, Kumar M et al (2021) Water spread mapping of multiple lakes using remote sensing and satellite data. Arab J Geosci 14:1–15

Deoli V, Kumar D, Kuriqi A (2022) Detection of water spread area changes in eutrophic lake using landsat data. Sensors 22:6827

Dou X, Fan X, Yunus AP et al (2021) Spatio-temporal evolution of glacial lakes in the Tibetan Plateau over the past 30 years. Earth Syst Sci Data Discuss 2021:1–31

Du Y, Zhang Y, Ling F et al (2016) Water bodies' mapping from Sentinel-2 imagery with modified normalized difference water index at 10-m spatial resolution produced by sharpening the SWIR band. Remote Sens (Basel) 8:354

Emami H, Zarei A (2021) Modelling lake water's surface changes using environmental and remote sensing data: a case study of lake urmia. Remote Sens Appl 23:100594

Fanton J-P (2021) Convolution and deconvolution: two mathematical tools to help performing tests in research and industry. Int J Metrol Qual Eng 12:6

Feng L, Hou X, Zheng Y (2019) Monitoring and understanding the water transparency changes of fifty large lakes on the Yangtze Plain based on long-term MODIS observations. Remote Sens Environ 221:675–686

Feyisa GL, Meilby H, Fensholt R, Proud SR (2014) Automated water extraction index: a new technique for surface water mapping using landsat imagery. Remote Sens Environ 140:23–35

Gu K, Pati D, Dunson DB (2014) Bayesian multiscale modeling of closed curves in point clouds. J Am Stat Assoc 109:1481–1494. https://doi.org/10.1080/01621459.2014.934825

Hajizadeh Javaran MR, Rajabi MM, Kamali N et al (2023) Encoder–decoder convolutional neural networks for flow modeling in unsaturated porous media: forward and inverse approaches. Water (Basel) 15:2890

Han-Qiu XU (2005) A study on information extraction of water body with the modified normalized difference water index (MNDWI). Natl Remote Sens Bull 589–595

Hao X, Zhang G, Ma S (2016) Deep learning. Int J Semant Comput 10:417–439

Harvey KR, Hill GJE (2001) Vegetation mapping of a tropical freshwater swamp in the Northern Territory, Australia: a comparison of aerial photography, landsat TM and SPOT satellite imagery. Int J Remote Sens 22:2911–2925

Hennessy KJ, McInnes KL, Abbs DJ et al (2004) Climate change in New South Wales. Part 2, projected changes in climate extremes: consultancy report for the New South Wales Greenhouse Office. Sydney, NSW, Australia, New South Wales Greenhouse Office

Holben BN (1986) Characteristics of maximum-value composite images from temporal AVHRR data. Int J Remote Sens 7:1417–1434

Holdren GC (2014) The Salton Sea. An Uncertain Future for California's Largest Lake

Howe NR (2013) Document binarization with automatic parameter tuning. Int J Doc Anal Recognit (Ijdar) 16:247–258

Janiesch C, Zschech P, Heinrich K (2021) Machine learning and deep learning. Electron Markets 31:685–695

Keren D (2004) Topologically faithful fitting of simple closed curves. IEEE Trans Pattern Anal Mach Intell 26:118–123

Kingsford RT, Basset A, Jackson L (2016) Wetlands: conservation's poor cousins. Aquat Conserv 26:892–916

Kjelland ME, Swannack TM (2018) Salton Sea days of future past: modeling impacts of alternative water transfer scenarios on fish and bird population dynamics. Ecol Inf 43:124–145. https://doi.org/10.1016/j.ecoinf.2017.06.001

Laga H, Kurtek S, Srivastava A, Miklavcic SJ (2014) Landmark-free statistical analysis of the shape of plant leaves. J Theor Biol 363:41–52. https://doi.org/10.1016/j.jtbi.2014.07.036

Lang OI, Mallia D, McKenzie Skiles S (2023) The shrinking Great Salt Lake contributes to record high dust-on-snow deposition in the Wasatch Mountains during the 2022 snowmelt season. Environ Res Lett 18:64045. https://doi.org/10.1088/1748-9326/acd409

Li S, Sun D, Goldberg M, Stefanidis A (2013) Derivation of 30-m-resolution water maps from TERRA/MODIS and SRTM. Remote Sens Environ 134:417–430

Li S, Sun D, Goldberg MD et al (2018) Automatic near real-time flood detection using Suomi-NPP/VIIRS data. Remote Sens Environ 204:672–689

Liang L, Ma L, Qian L, Chen J (2020) An algorithm for out-of-distribution attack to neural network encoder. Preprint at https://doi.org/10.48550/arXiv.2009.08016.

Liu H, He G, Peng Y et al (2021a) Dynamic monitoring of surface water in the Tibetan Plateau from 1980s to 2019 based on satellite remote sensing images. J Mt Sci 18:2833–2841. https://doi.org/10.1007/s11629-020-6482-8

Liu Z, Herman JD, Huang G et al (2021b) Identifying climate change impacts on surface water supply in the southern Central Valley, California. Sci Total Environ 759:143429. https://doi.org/10.1016/j.scitotenv.2020.143429

Ma Y, Lin H, Sun H, Mo D (2009) Research on water information extraction based on CIWI model. Soil Water Conserv China 5:41–43

McFeeters SK (1996) The use of the normalized difference Water Index (NDWI) in the delineation of open water features. Int J Remote Sens 17:1425–1432

Mueller N, Lewis A, Roberts D et al (2016) Water observations from space: Mapping surface water from 25 years of landsat imagery across Australia. Remote Sens Environ 174:341–352

Mulligan T, Johnson ML, Veldhuis JD (1995) [4] methods for validating deconvolution analysis of pulsatile hormone release: luteinizing hormone as a paradigm. Methods in Neurosciences. Academic Press Inc, pp 109–129

Mundus S, Müssel C, Schmid F et al (2025) Binarize: binarization of one-dimensional data. Comprehensive R Archive Network (CRAN). Retrieved from https://cran.r-project.org/web/packages/Binarize/Binarize.pdf

Ozesmi SL, Bauer ME (2002) Satellite remote sensing of wetlands. Wetl Ecol Manag 10:381–402

Policelli F, Hubbard A, Jung HC et al (2018) Lake Chad total surface water area as derived from land surface temperature and radar remote sensing data. Remote Sens 10(2):252. https://doi.org/10.3390/rs10020252

Poudel U, Ahmad S, Stephen H (2021) Studying the intra-annual variability in surface area and volume of Salton Sea, California, using remote sensing-based water indices and GIS. World Environ Water Resour Congr 769–783. https://doi.org/10.1061/9780784483466.070

Press WH, Teukolsky SA, Vetterling WT, Flannery BP (1992) Numerical recipes in Fortran 77. The Art of Scientific Computing, V

Rocio V, Mosavi A, Ruiz R (2017) Deep learning: a review. Adv Intell Syst Comput 5

Sage D, Donati L, Soulez F et al (2017) DeconvolutionLab2: an open-source software for deconvolution microscopy. Methods 115:28–41

Santos CAG, Ghorbani MA, Abdi E et al (2024) Estimating water levels through smartphone-imaged gauges: a comparative analysis of ANN, DL, and CNN models. Water Resour Manage. https://doi.org/10.1007/s11269-024-04038-w

Șerban C, Maftei C, Dobrică G (2022) Surface water change detection via water indices and predictive modeling using remote sensing imagery: a case study of Nuntasi-Tuzla Lake, Romania. Water (Basel) 14:556

Shang S (2013) Lake surface area method to define minimum ecological lake level from level-area-storage curves. J Arid Land 5:133–142. https://doi.org/10.1007/s40333-013-0153-3

Srikanthan S, Bende-Michl U, Matic V et al (2022) Murray Basin—national hydrological projections assessment report. Bureau of Meteorolog y Report Melbourne

Sumiya E, Dorjsuren B, Yan D et al (2020) Changes in water surface area of the lake in the steppe region of Mongolia: a case study of Ugii Nuur Lake, Central Mongolia. (Water (Basel) 12)

Tan J, Yu D, Li Q et al (2020) Spatial relationship between land-use/land-cover change and land surface temperature in the Dongting Lake area, China. Sci Rep 10:9245

Thornber KK, Williams LR (2000) Closed curves in the analysis and segmentation of images. Perceptual Organization for Artificial Vision Systems, pp 249–263

Wang L, Zhang Y, Feng J (2005) On the euclidean distance of images. IEEE Trans Pattern Anal Mach Intell 27:1334–1339. https://doi.org/10.1109/TPAMI.2005.165

Wang X, Xiao X, Zou Z et al (2020) Tracking annual changes of coastal tidal flats in China during 1986–2016 through analyses of landsat images with google earth engine. Remote Sens Environ 238:110987

Wang Y, Shen Y, Guo Y et al (2022) Increasing shrinkage risk of endorheic lakes in the middle of farming-pastoral ecotone of Northern China. Ecol Indic 135:108523

Wang Z, Liu X, Li W et al (2023) Temporal and Spatial Variation Analysis of Lake Area Based on the ESTARFM Model: a case study of Qilu Lake in Yunnan Province, China. Water (Basel) 15:1800

Wang H, Liu J, Zeng S et al (2024) A novel landslide identification method for multi-scale and complex background region based on multi-model fusion: YOLO + U-Net. Landslides 21:901–917. https://doi.org/10.1007/s10346-023-02184-7

Wolfram Wolfram Net Encoder URL https://reference.wolframcloud.com/language/ref/netencoder/Image.html. Accessed 20 Sep 2024

Wu Q, Yue H, Liu Y, Hou E (2022) Geospatial quantitative analysis of the Aral Sea Shoreline changes using RS and GIS techniques. Earth Sci Inf 1–13

Xiang W, Yang P, Wang S et al (2018) Underwater image enhancement based on red channel weighted compensation and gamma correction model. Opto-Electronic Adv 1:180021–180024

Xu N, Ma Y, Zhang W, Wang XH (2021) Surface-water-level changes during 2003–2019 in Australia revealed by ICESat/ICESat-2 Altimetry and Landsat Imagery. IEEE Geosci Remote Sens Lett 18:1129–1133. https://doi.org/10.1109/LGRS.2020.2996769

Yang X, Zhao S, Qin X et al (2017) Mapping of urban surface water bodies from Sentinel-2 MSI imagery at 10 m resolution via NDWI-based image sharpening. Remote Sens (Basel) 9:596

Ying Y, Lin Y (2019) Inertial focusing and separation of particles in similar curved channels. Sci Rep 9:16575

Zhao R, Fu P, Zhou Y et al (2022) Annual 30-m big lake maps of the Tibetan Plateau in 1991–2018. Sci Data 9:164

Zhao T, Zhang X, Li Z et al (2023) Response of lake dynamics to climate change in the Qilian mountains from 1990 to 2020. Environ Resource Ecol J 4:55–64

Zheng B, Liu G, Wang H et al (2018) Study on the delimitation of the urban development boundary in a special economic zone: a case study of the central urban area of Doumen in Zhuhai, China. Sustainability 10(3):756. https://doi.org/10.3390/su10030756